# WDM-Enabled Multi-core Parallel Programmable Photonic Signal Processor

Zihang Yang[1,3,5], Yunlong Li[1,3,5], Shuang Zheng[1,3,4,*], Senyu Zhang[1,3], Yifei Chong[1,3], Qi Tian[1,3], Li Shen[1], José Capmany[2], Ming Tang[1,3,4], Minming Zhang[1,3,4,*]

[1]*School of Optical and Electronic Information and Wuhan National Laboratory for Optoelectronics, Wuhan, Hubei 430074, China*

[2]*ITEAM Research Institute, Universitat Politècnica de València, 46022 Valencia, Spain*

[3]*National Engineering Research Center for Next Generation Internet Access System, Wuhan, Hubei 430074, China*

[4]*Optics Valley Laboratory, Wuhan, Hubei 430074, China*

[5]*These authors contributed equally: Zihang Yang, Yunlong Li*

[*] *email: zshust@hust.edu.cn; mmz@hust.edu.cn*

# Supplementary Section 1

### Operating Principle of the MRR-MZI

The MRR-MZI consists of a MZI formed by two 50:50 MMIs, incorporating thermal phase shifters on the straight arms and over-coupled MRRs coupled to both arms. These resonators introduce additional phase shifts at their resonance wavelengths, as illustrated in Fig. 1b-g. By detuning the resonance wavelengths of the two MRRs (WDM-on mode), a full 0-2π phase coverage can be achieved near resonance, enabling distinct switching states compared to off-resonance conditions. Conversely, when the resonance wavelengths are aligned (WDM-off mode), the differential phase shift vanishes, and identical switching states are maintained for both resonant and non-resonant wavelengths.

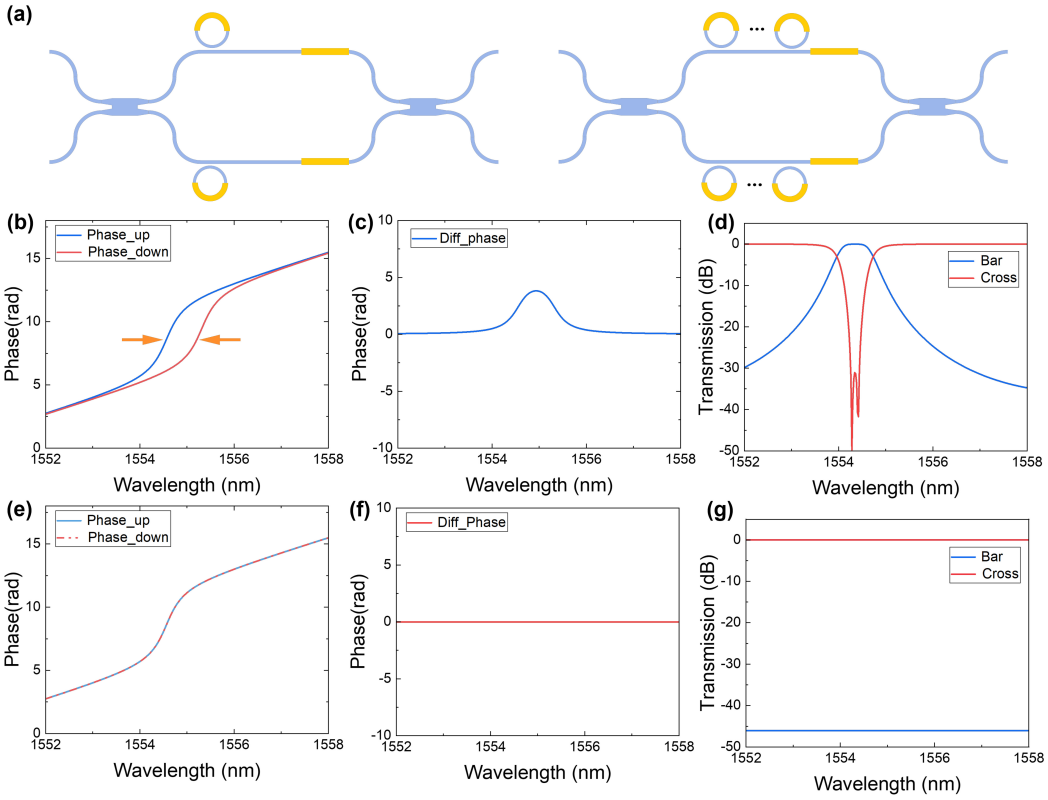


**Fig. 1 | Operating principle of MRR-MZI units. (a)** Schematic diagram of the MRR-MZI structure. **(b)** Additional phase shift introduced by the MRR at its resonant wavelength under the WDM-on condition. **(c)** Phase difference between the two arms of the MZI under the WDM-on condition. **(d)** Output spectrum of the MRR-MZI under the WDM-on condition. **(e)** Additional phase shift introduced by the MRR at its resonant wavelength under the WDM-off condition. **(f)** Phase difference between the two arms of the MZI under the WDM-off condition. **(g)** Output spectrum of the MRR-MZI under the WDM-off condition.

The MRR-MZI can be described using a transmission matrix formalism:

$$J(\omega)=\begin{pmatrix} t & jk \\ jk & t \end{pmatrix}\cdot\begin{pmatrix} \dfrac{t-ae^{-j(\beta L_u^{ring}+\Delta\varphi_u^{ring})}}{1-tae^{-j(\beta L_u^{ring}+\Delta\varphi_u^{ring})}}\cdot e^{-j(\beta L+\Delta\varphi_u)} & 0 \\ 0 & \dfrac{t-ae^{-j(\beta L_l^{ring}+\Delta\varphi_l^{ring})}}{1-tae^{-j(\beta L_l^{ring}+\Delta\varphi_l^{ring})}}\cdot e^{-j(\beta L+\Delta\varphi_l)} \end{pmatrix}\cdot\begin{pmatrix} t & jk \\ jk & t \end{pmatrix} \quad (1)$$

The phase shift introduced by thermal tuning is given by:

$$\Delta\varphi=\frac{2\pi L}{\lambda}\frac{dn_{eff}}{dT}\Delta T \quad (2)$$

Assuming ideal 50:50 splitting, the matrix simplifies to:

$$J(\omega)=\frac{1}{2}\begin{pmatrix} h_u-h_l & j(h_u+h_l) \\ j(h_u+h_l) & -h_u+h_l \end{pmatrix} \quad (3)$$

Where:

$$h_u = H_u(\omega)\cdot e^{-j(\beta L^{arm}+\Delta\varphi_u)} = \frac{t-ae^{-j(\beta L_u^{ring}+\Delta\varphi_u^{ring})}}{1-tae^{-j(\beta L_u^{ring}+\Delta\varphi_u^{ring})}}\cdot e^{-j(\beta L^{arm}+\Delta\varphi_u)} \tag{4}$$

$$h_l = H_l(\omega)\cdot e^{-j(\beta L^{arm}+\Delta\varphi_l)} = \frac{t-ae^{-j(\beta L_l^{ring}+\Delta\varphi_l^{ring})}}{1-tae^{-j(\beta L_l^{ring}+\Delta\varphi_l^{ring})}}\cdot e^{-j(\beta L^{arm}+\Delta\varphi_l)} \tag{5}$$

And the through and cross port transmissions are:

$$J_{Thru}(\omega) = J_{11}(\omega) = \frac{1}{2}(h_u - h_l) \tag{6}$$

$$J_{Cross}(\omega) = J_{21}(\omega) = \frac{j}{2}(h_u + h_l) \tag{7}$$

By tuning the MRR such that its resonance is slightly detuned from the target wavelength and establishing a π phase difference between the two arms, the switching state of the MRR-MZI is altered:

$$\Delta\varphi(\omega) = \arg[H_u(\omega)|_{\omega=\omega_{res}^u-\Delta\omega}] - \arg[H_l(\omega)|_{\omega=\omega_{res}^l+\Delta\omega}] + (\Delta\varphi_u - \Delta\varphi_l) = \pi \tag{8}$$

A continuous 0-to-2π phase shift at a given wavelength can be achieved by gradually tuning the resonance offset between the MRRs, thus allowing fully independent and reconfigurable switching control at that specific wavelength.

Extending the structure to include *N* MRR pairs, the transmission becomes:

$$J_{Thru}(\omega) = J_{11}(\omega) = \frac{1}{2}(h_u^{Total} - h_l^{Total}) \tag{9}$$

$$J_{Cross}(\omega) = J_{21}(\omega) = \frac{j}{2}(h_u^{Total} + h_l^{Total}) \tag{10}$$

Where：

$$h_u^{Total} = \prod_{i=1}^{N}\frac{t-ae^{-j(\beta L_u^{ring}+\Delta\varphi_{u,i}^{ring})}}{1-tae^{-j(\beta L_u^{ring}+\Delta\varphi_{u,i}^{ring})}}\cdot e^{-j(\beta L^{arm}+\Delta\varphi_u)} \tag{11}$$

$$h_l^{Total} = \prod_{i=1}^{N}\frac{t-ae^{-j(\beta L_l^{ring}+\Delta\varphi_{l,i}^{ring})}}{1-tae^{-j(\beta L_l^{ring}+\Delta\varphi_{l,i}^{ring})}}\cdot e^{-j(\beta L^{arm}+\Delta\varphi_l)} \tag{12}$$

Each MRR pair selectively controls a designated wavelength. When other MRRs are off-resonant from a given wavelength, their influence reduces to a fixed phase shift, yielding:

$$\sum_{n=1,n\neq i}^{N}\left\{\arg[H_{u,n}(\omega_i)]-\arg[H_{l,n}(\omega_i)]\right\}=const \tag{13}$$

$$\begin{aligned}\Delta\varphi(\omega_i)&=\sum_{n=1}^{N}\left\{\arg[H_{u,n}(\omega_i)]-\arg[H_{l,n}(\omega_i)]\right\}+(\Delta\varphi_u-\Delta\varphi_l)\\&=\arg[H_{u,n=i}(\omega_i)|_{\omega_i=\omega_{res}^{u}-\Delta\omega}]-\arg[H_{l,n=i}(\omega_i)|_{\omega_i=\omega_{res}^{l}+\Delta\omega}]+const+(\Delta\varphi_u-\Delta\varphi_l)\end{aligned} \tag{14}$$

Where $n$ denotes the index of the controllable wavelength.

This architecture allows for parallel and independent control of multiple wavelengths by varying the number of MRR groups.

**Wavelength routing flexibility**

The MZI selects output ports by inducing interference through the phase difference between its two arms. As the phase shifters operate over a broad spectrum, the MZI itself functions as a broadband device, maintaining consistent switching states across a wide wavelength range. However, when a topological network is required to handle multiple wavelength channels for distinct tasks, this uniform switching behavior imposes limitations on signal processing flexibility. A single MZI unit cannot independently configure switching states for different wavelengths, thereby restricting functional reconfigurability. Although wavelength selectivity can be introduced by incorporating resonant structures into the network, this often requires additional unit cells, leading to increased processor footprint and additional optical loss, ultimately compromising the chip area available for other operations.

We propose a metric to quantify the flexibility of programmable photonic processors in multi-wavelength scenarios:

$$Eval=\frac{\lambda}{N\times Loss} \tag{15}$$

where λ is the number of separable wavelengths, $N$ the number of basic units required, and $Loss$ the insertion loss per unit. This metric characterizes the overhead involved in implementing wavelength-selective functionality within a programmable photonic network.

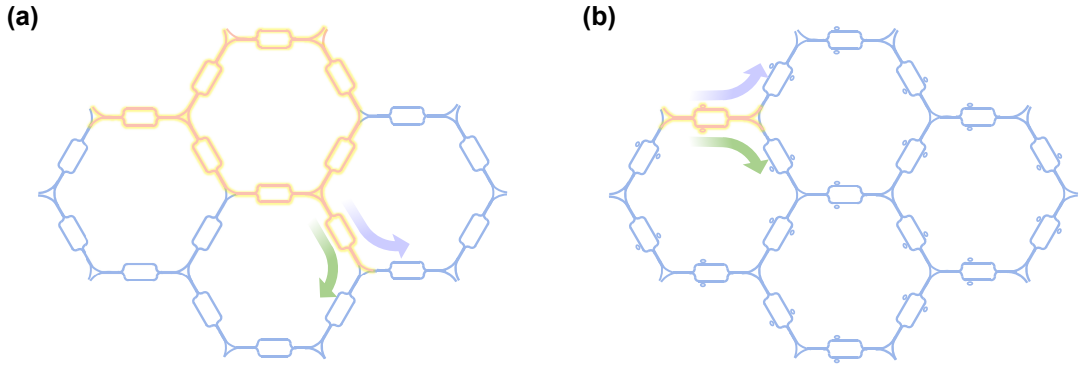


**Fig. 2 | Comparison between MZI-based and MRR-MZI-based programmable photonic processors. (a)** Required configuration of an MZI-based programmable photonic processor for separating two wavelengths**. (b)** Required configuration of an MRR-MZI-based programmable photonic processor for separating two wavelengths.

As shown in Figs. 2a, b, we compare MZI-based and MRR-MZI-based processors. To separate two wavelengths, MZI-based systems require asymmetric configurations, while MRR-MZI structures achieve the same with a single unit due to the wavelength selectivity of MRR. Assuming 0.5 dB insertion loss per MZI and 0.2 dB additional loss per MRR:

$$Eval_{MZI} = \frac{2}{8 \times 0.5} = 0.5 \tag{16}$$

$$Eval_{MRR-MZI} = \frac{2}{1 \times (0.2 + 0.5)} = 2.86 \tag{17}$$

With increasing wavelength channels, the proposed design achieves scalable wavelength separation via a linear combination of MRR-MZI units, without enlarging the processor footprint, thereby improving system flexibility and enabling more sophisticated photonic configurations.

**Thermo-optic Response of the MRR-MZI**

The basic unit integrates four TiN heaters distributed across the MRR and the straight arms of the MZI to enable phase tuning. By electrically grounding the TiN heaters in a common configuration, the number of pad is reduced. We measured the static tuning curves of both the MRR phase shifters and the straight-arm phase shifters, and compared the power consumption required to achieve a π phase shift. The MRR phase shifter requires only 4.313 mW to realize a π phase shift, whereas the straight-arm phase shifter requires 20.709 mW, indicating that the MRR-based phase modulation is significantly more power-efficient (Fig. 3a).

Furthermore, we characterized the transient response of the TiN heaters under square-wave modulation at frequencies of 5 kHz, as shown in Figs. 3b, c. The MRR exhibits rise and fall times (10%–90%) of 21.4 μs and 22 μs, respectively, while the MZI shows slightly different values of 21.6 μs and 20 μs.

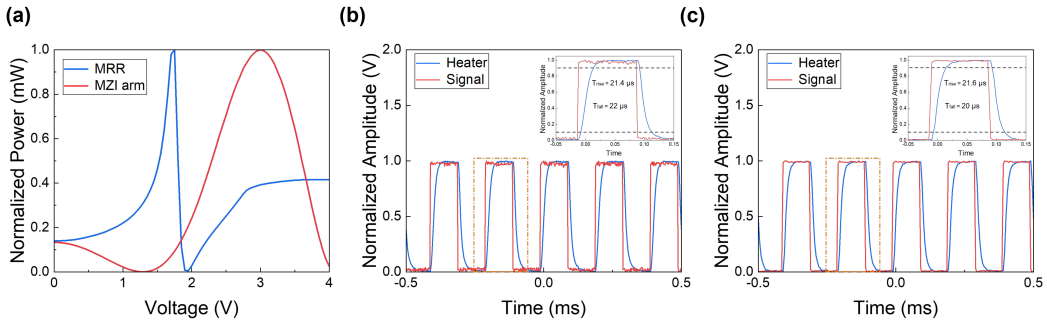


**Fig. 3 | Thermal response of the MRR-MZI. (a)** Static tuning curve of the MRR and straight-arm phase shifter. **(b)** Dynamic modulation response of the MRR at a modulation rate of 5 kHz. **(c)** Dynamic modulation response of the MZI at a modulation rate of 5 kHz.

# Supplementary Section 2

MRR inevitably introduce losses at resonance. When only one arm couples to a MRR, overall loss is reduced but the phase coverage becomes insufficient for full 0-2π modulation, degrading extinction ratio and limiting function (e.g. in matrix operations).

With the basic unit transmission matrix:

$$J(\omega)=\frac{1}{2}\begin{pmatrix}1 & j\\ j & 1\end{pmatrix}\cdot\begin{pmatrix}\dfrac{t-ae^{-j(\beta L+\Delta\varphi_u^{ring})}}{1-tae^{-j(\beta L+\Delta\varphi_u^{ring})}} & 0\\ 0 & 1\end{pmatrix}\cdot\begin{pmatrix}1 & j\\ j & 1\end{pmatrix} \tag{18}$$

the extinction ratio at the Cross state is:

$$ER=10\lg(\frac{P_{\max}}{P_{\min}})=10\lg(\frac{|h_u+h_l|^2{}_{\max}}{|h_u+h_l|^2{}_{\min}})=20\lg\left(\frac{(1-ta)(1+a)}{(1+ta)(1-a)}\right) \tag{19}$$

When both the upper and lower arms are coupled to MRRs and the phase difference equals π, the following relation holds:

$$\begin{aligned}|h_u+h_l|^2{}_{\min}&=\left|\frac{t-ae^{-j(\beta L+\Delta\varphi_u^{ring})}}{1-tae^{-j(\beta L+\Delta\varphi_u^{ring})}}+\frac{t-ae^{-j(\beta L+\Delta\varphi_l^{ring})}}{1-tae^{-j(\beta L+\Delta\varphi_l^{ring})}}\right|^2_{\min}\\&=\left|H_u(\omega)e^{-j\theta^u(\omega)}|_{\omega=\omega_{res}^u-\Delta\omega}+H_l(\omega)e^{-j(\theta^l(\omega))}|_{\omega=\omega_{res}^l-\Delta\omega}\right|^2\\&=\left|H_u(\omega)e^{-j\theta^u(\omega)}+H_u(\omega)e^{-j(\theta^u(\omega)-\pi)}\right|^2\\&=0\end{aligned} \tag{20}$$

Then：

$$ER=10\lg(\frac{P_{\max}}{P_{\min}})=10\lg(\frac{|h_u+h_l|^2{}_{\max}}{|h_u+h_l|^2{}_{\min}})=10\lg\left(\frac{|h_u+h_l|^2{}_{\max}}{0}\right)=\infty \tag{21}$$

By fixing the MRR loss coefficient, we performed simulations to investigate the variation of the extinction ratio in the Cross state of a single-arm coupled MRR as the amplitude transmission coefficient varies. The results are shown in Fig. 4. It can be observed that the extinction ratio of the single-arm coupled MRR is significantly affected by the MRR loss. In contrast, when both the upper and lower arms are coupled with MRRs, the extinction ratio becomes largely insensitive to the loss.

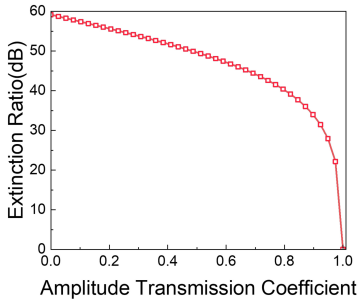

**Fig. 4 | Extinction ratio of single-MRR-assisted MZI versus MRR coupling coefficient.**

# Supplementary Section 3

We employ a commercial C-band 4-channel tunable laser with a maximum output power of 15.5 dBm. Electrical signals from a BERT are modulated onto the optical carrier via a commercial MZM driven by an RF amplifier. Signals are detected at different output ports of the processor while varying the laser wavelength. At 25 Gbps, we configure the processor as a demultiplexer and capture NRZ eye diagrams (Fig. 5):

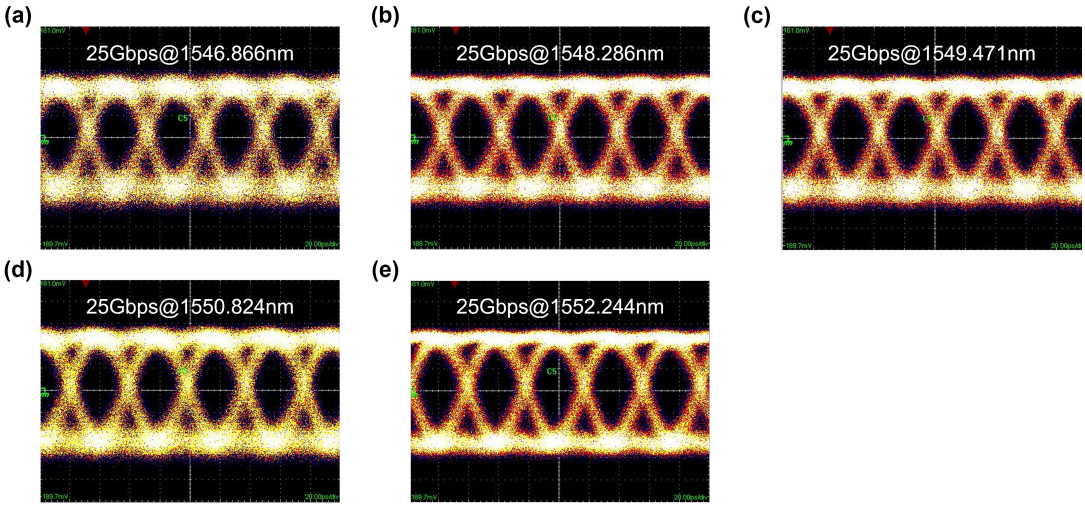


**Fig. 5 | Output eye diagrams at 0 dBm input power. (a)** Eye diagram at port 1. **(b)** Eye diagram at port 2. **(c)** Eye diagram at port 3. **(d)** Eye diagram at port 4. **(e)** Eye diagram at port 5.

Due to limitations in the optical source output power, BER measurements were conducted by increasing the output power of the EDFA. While the EDFA provides the necessary signal amplification, it also introduces and amplifies noise. As a result, the measured BER curves deviate from the conventional behavior, showing diminished improvement in BER at higher output power levels.

# Supplementary Section 4

To clarify how dual-wavelength control is achieved with only a single pair of coupled MRRs, we provide a more detailed explanation here. In theory, fully independent control over two wavelengths would require two sets of MRRs, each capable of providing a complete 0–2π phase tuning range. However, when the MRR–MZI incorporates an additional straight-arm phase shifter, the control mechanism changes fundamentally. In this configuration, the straight-arm heater functions as a wavelength-independent phase shifter, whereas each MRR serves as a wavelength-dependent phase shifter, introducing wavelength-selective phase responses. The coexistence of these two types of phase shifters effectively increases the degree of freedom in wavelength-domain control.

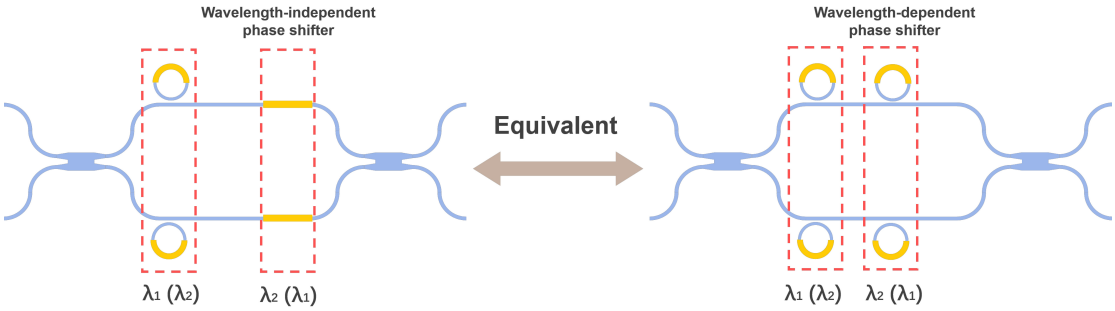


**Fig. 6 | Schematic illustration of the wavelength control strategie for the MRR-MZI unit.**

As illustrated in Fig. 6, this hybrid phase-shifting scheme enables dual-wavelength operation using only one pair of coupled MRRs. Specifically, the MRRs are used solely as wavelength-dependent phase shifters to control one wavelength, while the straight-arm phase shifter provides phase tuning for the other. Although tuning the straight-arm phase shifter introduces a minor phase perturbation to the wavelength controlled by the MRRs, this effect can be readily compensated by fine-tuning the MRR resonances, thus achieving independent phase control at both wavelengths.

# Supplementary Section 5

Although MRR-MZIs exhibit similar spectral profiles as MZIs in WDM-off mode, the abrupt phase transitions at resonance persist. As a result, even in WDM-off mode, resonant and non-resonant wavelengths incur different delays-posing challenges for dual-wavelength delay networks.

To enable a dual-wavelength parallel delay network configuration, the programmable photonic processor must function equivalently as multiple independent delay networks. In this scenario, the fundamental building block the MRR-MZI must assume different switching states at different wavelengths. This necessitates configuring the MRR-MZI in the WDM-on mode, wherein the resonance wavelength of the MRRs aligns with the optical carrier wavelength. Compared to the off-resonant regime, the on-resonant configuration induces a larger group delay.

Focusing on wavelength-specific switching control, when only the MRR is used for tuning without employing the phase shifters on the straight arms the MRR-MZI exhibits a Bar state when the MRR resonance is detuned from the signal wavelength, and a Cross state when they are aligned. This approach is sufficient for applications requiring only spectral routing. However, in delay networks, such a configuration results in a significant mismatch in the delay values between the Bar and Cross states, as shown in Figs. 7a–c. Consequently, the flexibility of the delay network is limited, since each path must include an equal number of Cross and Bar states to ensure precise delay matching.

The underlying cause of this delay mismatch lies in the fact that the resonance wavelengths of the MRR differ under different switching states. To address this issue, we propose a method to switch the state of the MRR-MZI without altering the MRR resonance wavelengths. This approach leverages the phase shifter on the straight arm to bias the MRR-MZI to a 50:50 splitting condition. By detuning the resonance wavelengths of the two MRR s, the MRR-MZI exhibits a Bar state near resonance; a voltage-induced interchange of the MRR s' resonance wavelengths result in a Cross state. Under this scheme, the group delay remains consistent between the Bar and Cross states, as illustrated in Figs. 7d–f. This method effectively overcomes the limitations imposed by delay imbalance in conventional configurations.

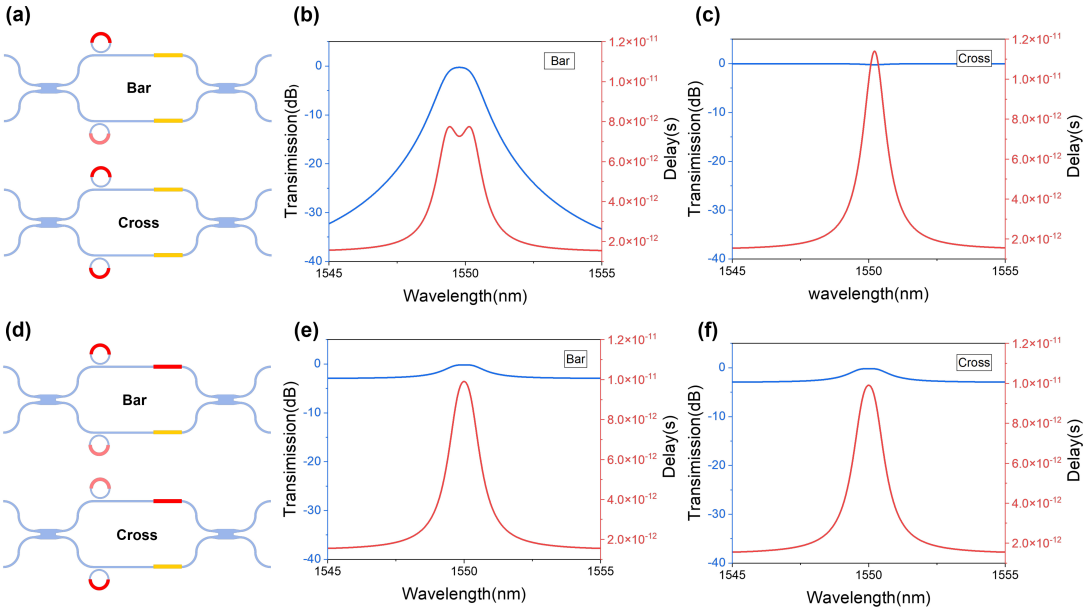


**Fig. 7 | Time delay characteristics of the MRR-MZI under different tuning conditions. (a)** Tuning the MRR only. **(b)** Output spectrum and delay spectrum at the bar port. **(c)** Output spectrum and delay spectrum at the cross port. **(d)** Simultaneous tuning of the MRR and the straight-arm phase shifter. **(e)** Output spectrum and delay spectrum at the bar port. **(f)** Output spectrum and delay spectrum at the cross port.

In addition, the basic unit within the delay network also performs optical splitting for different paths. Although different splitting ratios can be achieved by tuning the resonance wavelengths of the MRRs, this approach leads to variations in the group delay of the MRR-MZI at different splitting ratios, as illustrated in Fig. 8:

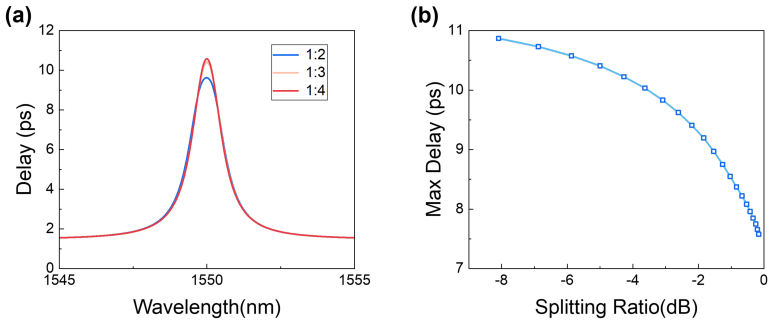


**Fig. 8 | Delay characteristics of the MRR-MZI at its resonance wavelength for various power splitting ratios. (a)** Measured time delays with splitting ratios of 1:2, 1:3, and 1:4. **(b)** Variation of the maximum delay with respect to the splitting ratio.

Taking as an example a delay network with a unit delay difference of one BU and 4 delay paths, each MRR-MZI provide a delay of $T$, with subscripts indicating the switching state of each basic unit. The delay of each path can then be expressed as:

$$\begin{aligned} Out_1 &= 4T_{Bar} + T_{1:4} \\ Out_2 &= 4T_{Bar} + T_{1:4} + T_{1:3} \\ Out_3 &= 4T_{Bar} + T_{1:4} + T_{1:3} + T_{1:2} \\ Out_4 &= 4T_{Bar} + T_{1:4} + T_{1:3} + T_{1:2} + T_{Cross} \end{aligned} \tag{22}$$

It is apparent that the MRR-MZI serves a dual role in the network, both as a delay element and a splitter. While the splitting ratio can be modulated by tuning the MRR resonances, this tuning inevitably alters the delay, degrading the overall delay performance. To address this challenge, we propose adding a compensation stage after each path, consisting of two MRR-MZI units, to align the delays. By tuning the switching states of the unit cells in the compensation stage, the delay can satisfy the following relation:

$$\begin{aligned} Out_1 &= 4T_{Bar} + T_{1:4} + (T_{1:3} + T_{1:2})_{comp} \\ Out_2 &= 4T_{Bar} + T_{1:4} + T_{1:3} + (T_{1:2} + T_{Bar})_{comp} \\ Out_3 &= 4T_{Bar} + T_{1:4} + T_{1:3} + T_{1:2} + (T_{Bar} + T_{Bar})_{comp} \\ Out_4 &= 4T_{Bar} + T_{1:4} + T_{1:3} + T_{1:2} + T_{Cross} + (T_{Bar} + T_{Bar})_{comp} \end{aligned} \tag{23}$$

To ensure consistent optical power across all paths, the MRR resonance wavelengths in the compensation stage are fixed, while the phase shifters on the straight arms are tuned to maintain the desired Bar or Cross state at the compensation wavelength, as shown in Fig. 9. This ensures a constant delay difference $T_{Bar}$ among all paths.

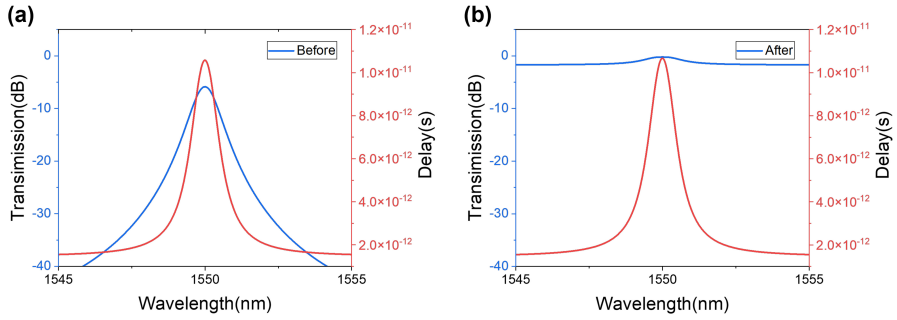


**Fig. 9 | Principle of the compensation stage in MRR-MZI configuration. (a)** Spectral and delay responses when only delay is compensated without correcting output power. **(b)** Spectral and delay responses when both delay and output power are compensated simultaneously.

When the number of MRR pairs coupled to the MZI is two, the designed programmable photonic processor can realize a parallel dual-beamforming network. The beam steering configuration scheme is illustrated in Fig. 10.

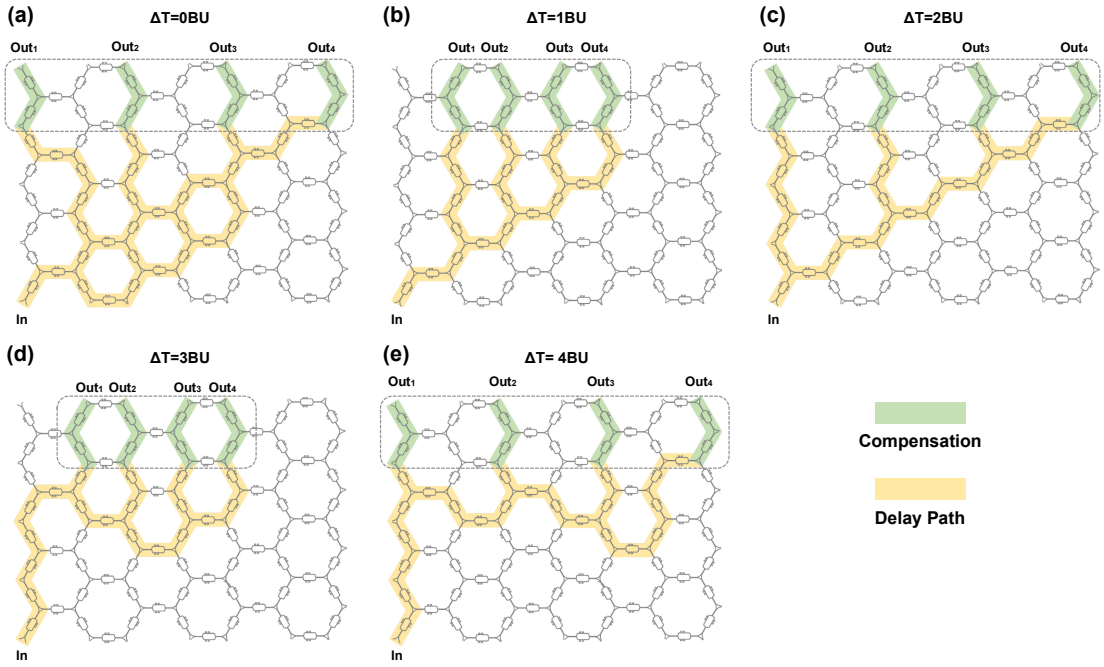


**Fig. 10 | Path configurations corresponding to different delay differences. (a)** Path configuration with a delay difference of 0 BU. **(b)** Path configuration with a delay difference of 1 BU. **(c)** Path configuration with a delay difference of 2 BU. **(d)** Path configuration with a delay difference of 3 BU. **(e)** Path configuration with a delay difference of 4 BU.